Computer-Aided Design (CAD) of Mn(II) Complexes: Superoxide Dismutase Mimetics with Catalytic Activity Exceeding the Native Enzyme

Karl Aston,[#] Nigam Rath,[‡] Arati Naik,[†] Urszula Slomczynska,[†] Otto F. Schall,[†] and Dennis P. Riley*[,†]

Pharmacia Corporation (BB4M), 700 Chesterfield Parkway North, Chesterfield, Missouri 63017, The University of Missouri, St. Louis, Missouri 63121, and MetaPhore Pharmaceuticals, Inc., 1910 Innerbelt Business Center Drive, St. Louis, Missouri 63114

Received August 22, 2000

New Mn(II) macrocyclic pentaamine complexes derived from the biscyclohexyl-pyridine complex, M40403 ([manganese(II)dichloro{(4R,9R,14R,19R)-3,10,13,20,26-pentaazatetracyclo[20.3.1.0.^{4,9}0^{14,19}]hexacosa-1(26),-22(23),24-triene}]), are described here. The complex M40403 was previously shown to be a superoxide dismutase (SOD) catalyst with rates for the catalytic dismutation of superoxide to oxygen and hydrogen peroxide at pH = 7.4 of $1.2 \times 10^{+7}$ M^{-1} s^{-1}.[1] The use of the computer-aided design paradigm reported previously for this class of Mn(II) complexes[2,3] led to the prediction that the 2*S*,21*S*-dimethyl derivative of M40403 should possess superior catalytic SOD activity. The synthesis of this new macrocyclic Mn(II) complex, [manganese(II)dichloro{2*S*, 21*S*-dimethyl-(4R,9R,14R,19R)-3,10,13,20,26-pentaazatetracyclo[20.3.1.0.^{4,9}0^{14,19}]hexacosa-1(26),22(23),24-triene}], **5**, was accomplished via a high yield template condensation utilizing the linear tetraamine, *N*,*N*′-Bis-{(1*R*,2*R*)-[2-(amino)]cyclohexyl}-1,2-diaminoethane, **1**, 2,6-diacetylpyridine, and $MnCl_2$ to form the macrocyclic diimine complex, **2**, which then is reduced. The two other possible dimethyl diastereomers of **5** (2*R*,21*R*-dimethyl, **3**, and 2*R*,21*S*-dimethyl, **6**) were also prepared via reduction of the diimine complex **2**. Two of these complexes, **3** and **5**, were characterized by X-ray structure determination confirming their absolute stereochemistry as 2*R*,21*R*-dimethyl and 2*S*,21*S*-dimethyl, respectively. The results of the MM calculations which predict that the 2*S*,21*S*-dimethyl complex, **5**, should be a high activity catalyst and that the 2*R*,21*R*-dimethyl complex, **3**, should have little or no catalytic activity are presented. The catalytic SOD rates for these complexes are reported for each of these complexes and a correlation with the modeling predictions is established showing that 2*R*,21*R*-complex, **3**, has no measurable catalytic rate, while the 2*R*,21*S* complex, **6**, is identical to M40403, and the 2*S*,21*S*- complex, **5**, possesses a very fast rate at pH = 7.4 of $1.6 \times 10^{+9}$ M^{-1} s^{-1} exceeding that of the native mitochondrial MnSOD enzymes.

Introduction

Low molecular weight catalysts which mimic a natural enzymatic function (*synzymes)* have potential utility for the treatment of diseases characterized by the overproduction of potentially deleterious metabolic byproducts. One such undesired metabolic by-product arises from our use of molecular oxygen as the penultimate oxidant for metabolizing food stores. The one electron reduction product of oxygen, superoxide, is formed from a large number of sources, including normal cellular respiration, activated polymorphonuclear leukocytes, endothelial cells, and mitochondrial electron flux.[4] It has been implicated as playing a major role in the generation and propagation of numerous disease states. It has been a target in our efforts[5] and those of other groups[6] to develop highly active and stable metal complexes which could be utilized as human pharmaceutical agents.

Our discovery that pentaaza macrocyclic ligand complexes of manganese(II) are functional mimics of superoxide dismutase (SOD) enzymes,[7] and our subsequent studies on the mechanism,[8] led us to a level of understanding which made it possible for us to develop a computer-aided design paradigm based on molecular mechanics (MM) which provides a way to ascertain

* To whom correspondence should be addressed.
[†] MetaPhore Pharmaceuticals.
[‡] The University of Missouri.
[#] Pharmacia Corporation.

(1) (a) Salvemini, D.; Wang, Z.-Q.; Zweier, J.; Samouilov, A.; Macarthur, H.; Misko, T.; Currie, M.; Cuzzocrea, S.; Sikorski, J.; Riley, D. *Science* **1999**, *286*, 304. (b) Macarthur, H.; Westfall, T. C.; Riley, D. P.; Misko, T. P.; Salvemini, D. *PNAS* **2000**, *97*(17), 9753−9758.
(2) Riley, D. P.; Henke, S. L.; Lennon, P. J.; Aston, K. *Inorg. Chem.* **1999**, *38*, 1908.
(3) Riley, D. P. Rational design of synthetic enzymes and their potential utility as human pharmaceuticals: development of Mn(II)-based superoxide dismutase mimics. In *Advances in Supramolecular Chemistry*; JAI Press: London, 1999; Vol. 6, pp 217−244.
(4) (a) McCord, J. M.; Fridovich, I. *J. Biol Chem.* **1969**, *244*, 6049. (b) Fridovich, I. *J. Biol. Chem.* **1989**, *264*, 7761.
(5) (a) Riley, D. P.; Weiss, R. H. *CATTECH* **1997**, *1*, 41. (b) Weiss, R.; Riley, D. P. *Drugs Future* **1996**, *21*(4), 383−389. c) Salvemini, D.; Riley, D. P. *Cell. Mol. Life Sci.* **2000**, *57*(1), 1489−92. (d) Salvemini, D.; Riley, D. P. *Drugs Future* **2000**, *25*(10), 1027−1033.
(6) (a) Fridovich, I. *J. Biol. Chem.* **1997**, *272*(30), 18515. (b) Doctrow, S. R.; Huffman, K.; Marcus, C. B.; Malfroy, B. *Adv. Pharmacol.* **1997**, *38*, 2247.
(7) (a) Riley, D. P.; Weiss, R. H. *J. Am. Chem. Soc.* **1994**, *116*, 387. (b) Hardy, M. M.; Flickinger, A. G.; Riley, D. P.; Weiss, R. H.; Ryan, U. S. *J. Biol. Chem.* **1994**, *269*, 18535. (c)Weiss, R. H.; Fretland, D. J.; Baron, D. A.; Ryan, U. S.; Riley, D. P. *J. Biol. Chem.* **1996**, *271*(42), 26149−26156.
(8) (a) Riley, D. P.; Henke, S. L.; Lennon, P. J.; Weiss, R. H.; Neumann, W. L.; Rivers, W. J., Jr.; Aston, K. W.; Samples, K. R.; Rahman, H.; Ling, C.; Shieh, J.; Busch, D. H.; Szulbinski, W. *Inorg. Chem.* **1996**, *35*, 5213−5231. (b) Riley, D. P.; Lennon, P. J.; Neumann, W. L.; Weiss, R. H. *J. Am. Chem. Soc.* **1997**, *119*(28), 6522−6528.

10.1021/ic000958v CCC: $20.00
Published on Web 03/13/2001

how substituents on the macrocycle effect catalytic rates.[2] In this class of macrocycles, the ligand dictates the geometry about the spherically symmetrical Mn(II) ion. Thus, the substituents on the macrocycle (i.e., their stereochemistry, position, and the number and type) will dictate the geometry of the Mn(II) complex. Our studies on mechanism further revealed that catalytic activity correlates with the ability of the Mn(II) complex to adopt the desired geometry of the Mn(III) ion formed during the rate-determining step of the catalytic cycle. Thus, if the ligand substituents force a folded geometry about the Mn(II) ion preorganizing the Mn(II) to resemble the shape of the resultant oxidized Mn(III) complex, faster catalytic rates will be achieved.[2]

Previously, we reported that M40403 is an SOD mimetic with significant efficacy in animal models of inflammation and reperfusion injury.[1] This complex has remarkably high kinetic and thermodynamic stability with regard to dissociation and is oxidatively stable as well. In fact, our preliminary metabolism studies revealed that the compound is not actually metabolized but is excreted intact with no dissociation in vivo. This stability profile is desirable for a metal-based drug and is one which we wanted to capture in our attempts to design an improved, more catalytically active, derivative.

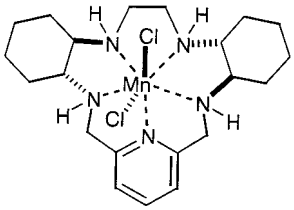

M40403

Another important advantage which the M40403 ligand framework possesses is its ease of synthesis via a template route which makes it possible to construct a fifteen-membered ring system with the metal in place in one step in very good yield with high reactant concentrations.[1,9,10]

Given the very desirable combination of properties (including metabolic stability, catalytic activity, selectivity, potential ease of synthesis, etc.) that the M40403 complex possesses, we set out to determine whether CAD could guide us to an even better, more active, SOD catalyst employing this ligand framework. Employing the molecular mechanics (MM) tools which we have developed and which allow us to correlate catalytic SOD activity with a substituent's size, stereochemistry, and location on the macrocyclic ligand, we determined that the 2*S*,21*S*-dimethyl substituted derivative of M40403 should possess a greatly enhanced catalytic SOD activity, while the *R*,*R*-dimethyl complex should be of very low catalytic activity. We describe in this paper not only the modeling studies which led to these and other predictions but also the synthesis of three new diastereomeric 2,21-dimethyl substituted derivatives of M40403. All three new complexes (**3**, **5**, and **6**) can be constructed in high yield via a template methodology utilizing 2,6-diacetylpyridine in place of 2,6- pyridinedialdehyde to generate the bisimine precursor complex, **2** (Scheme 1).[1,10] In addition to describing the results of modeling calculations for M40403 and its three new dimethyl diastereomeric derivatives, we report their characterization (including the X-ray structure determination for the complexes **3** and **5**, confirming the stereochemical assignments for these three diastereomeric complexes) and the results of catalytic rate constant determinations (obtained by the stopped flow kinetic analysis of the superoxide dismutase catalysis for each of these new complexes[11]) which are in agreement with the modeling predictions.

Scheme 1

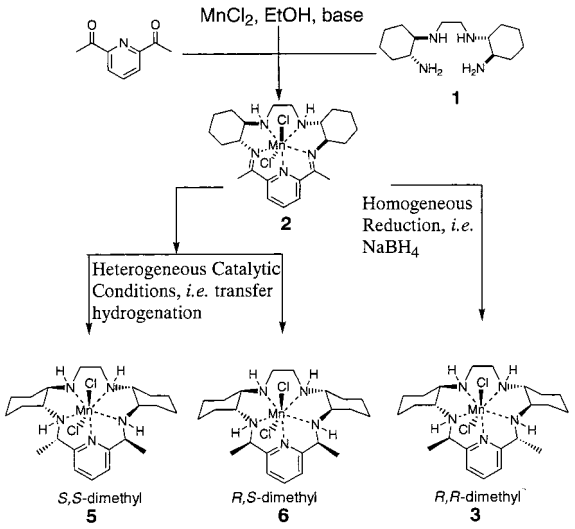

Experimental Section

Materials. 2,6-Diacetylpyridine (99%), ammonium formate (97%), sodium borohydride (98%), EtOH (abs., anhydrous), palladium on activated carbon (3 wt % Pd), 2-propanol (27,049-0), and trifluoroacetic acid (T6508) were purchased from Aldrich (Milwaukee, WI). UV grade acetonitrile (015-4) and water (AH365-4) were obtained from Burdick & Jackson (Muskegon, MI). 2-(*N*-morpholino)-ethanesulfonic acid (475893) and its sodium salt (475894) were purchased from Calbiochem (La Jolla, CA). Manganese(II) chloride (Ultra dry, 99.998% Mn content) was purchased from Alfa Æsar. Potassium hydroxide (KOH content 86.9%), lithium chloride, and all other solvents (HPLC grade unless otherwise indicated) were purchased from Fisher Scientific and were of the finest grade available. Uniplate thin-layer chromatography plates (Silica Gel GF, catalog #02521) were purchased from Analtech, Inc., in Newark, DE. Davisil silica gel (grade 1740, type 60A, 170−400 mesh) and Bakerbond Octadecyl (C_{18}) 40 μm silica gel were purchased from Fisher Scientific.

Methods. Combustion analysis was performed by Atlantic Microlab in Norcross, GA. HPLC was carried out using a Waters YMC ODS-AQ S5 120 Å (4.6 mm × 50 mm) HPLC column. Solvent system A was 0.5 M aq NaCl. Solvent system B was 1:4 water/CH_3CN. A gradient of 10−50% or 10−100% system B over 9 min was used at a flow rate of 3 mL/min and UV detection at 265 nm. For preparative HPLC the same column was employed but in a (20 mm × 50 mm) size.

Kinetic stabilities of the new complexes were determined using the methodology which was described in detail previously[1,8] and which is described here in general terms. Three buffer solutions (pH 3.50, 3.70, and 4.38) were prepared using 2-(*N*-morpholino)-ethanesulfonic acid (HMES) and its sodium salt (NaMES). Samples of each complex were dissolved in 25 mL of the 200 mM MES buffer solutions at various pHs over the range 3.5−4.5 and the resulting 300 μM samples were analyzed over time by HPLC. Conditions for analysis were 20% acetonitrile in 80% 0.05% TFA in water, 2 mL/min, and 20 μL injection. When a sufficient number of points (>3 half-lives) had been collected, the data were plotted (time in seconds vs the natural log of the area) and the slope (equal to the negative of the proton dependent dissociation

(9) Alcock, N. W.; Liles, D. C.; McPartlin, M.; Tasker, P. A. *J. C. S. Commun.* **1974**, 727.
(10) Aston, K. W.; Franklin, G. W.; Lennon, P. L.; Rath, N.; Neumann, W. L. *Org. Lett.*, submitted.
(11) (a) Weiss R. H.; Flickinger, A. G.; Rivers W. J.; Hardy, M. M.; Aston, K. W.; Ryan, U. S.; Riley, D. P. *J. Biol. Chem.* **1993**, *268*(31), 23049−23054. (b) Riley, D. P.; Rivers, W. J.; Weiss, R. H. *Anal. Biochem.* **1991**, *196*(2), 344−349.

Table 1. Crystal Data and Structure Refinement for **3**

empirical formula	$C_{23}H_{41}C1_2MnN_5O$
fw	529.45
temp	298(2) K
wavelength	0.71073 Å
cryst syst	orthorhombic
space group	$P2_12_12_1$
unit cell dimensions	$a = 8.42910(10)$ Å, $\alpha = 90°$ $b = 16.6077(2)$ Å, $\beta = 90°$ $c = 18.6214(2)$ Å, $\gamma = 90°$
V, Z	2606.77(5) Å^3, 4
D (calcd)	1.349 mg/m^3
absorption coefficient	0.736 mm^{-1}
F(000)	1124
cryst size	0.30 mm × 0.40 mm × 0.40 mm
∪ range for data collection	1.64−28.00°
limiting indices	$-11 \le h \le 11$, $-23 < k < 23$, $-26 \le 1 \le 26$
reflns collected	24 823
independent reflns	6277 ($R_{int} = 0.0270$)
absorption correction	none
Refinement method	full matrix least-squares on F^2
data/restraints/parameters	6275/0/453
goodness-of-fit on F^2	1.073
final R indices [$I > 2\sigma(I)$]	R1 = 0.0235, wR2 = 0.0497
R indices (all data)	R1 = 0.0272, wR2 = 0.0515
absolute structure parameter	0.001(10)
largest diff peak and hole	0.147 and −0.122 eÅ^{-3}

constant, k_{obs}) was determined. The pH of the final solution was checked (to ensure that dissociation of the complex had not caused any drastic pH changes), and the concentration of hydrogen ion, [H$^+$], at each pH was graphed versus the k_{obs}. The slope of this graph is the second-order proton dependent dissociation constant, k_{diss}.

The method used to determine the superoxide dismutase catalytic activity is based on the stopped flow kinetic assay described previously.[11]

Molecular Mechanics. The molecular mechanics (MM) computations were carried out using the mechanics software implemented on a Tektronix CAChe workstation using code based on Allinger's MM-2 molecular mechanics code with extensions provided by the CAChe Group.[12] Details on the methods as applied to the Mn(II) complexes of the type reported herein were described previously in ref 2.

X-ray Crystal Structure Determination for 3 and 5. Crystals of appropriate dimensions were mounted on glass fibers in random orientations. Preliminary examination and data collection were performed using a Bruker SMART Charge Coupled Device (CCD) Detector single-crystal X-ray diffractometer using a graphite-monochromated Mo Kα radiation ($\lambda = 0.71073$ Å) source equipped with a sealed tube X-ray source at 25 °C for **3** and −50 °C for **5**. Preliminary unit cell constants were determined with a set of 45 narrow frames (0.3° in $\bar{\omega}$) scans. A typical data set collected consists of 4028 frames of intensity data collected with a frame width of 0.3° in $\bar{\omega}$ and a counting time of 10 or 15 s/frame at a crystal to detector distance of 4.930 cm. The double pass method of scanning was used to exclude any noise. The collected frames were integrated using an orientation matrix determined from the narrow frame scans. The SMART and SAINT software packages (Bruker Analytical X-ray, Madison, WI, 1997) were used for data collection and data integration. Analysis of the integrated data did not show any decay. Final cell constants were determined by a global refinement of strong reflections from the actual data collection (number of reflections used was ≤ 8192 ($\theta < 25.0°$)). Collected data were corrected for systematic errors using SADABS based upon the Laue symmetry using equivalent reflections.[13] Crystal data and intensity data collection parameters are listed in Tables1 and 5 for **3** and **5**, respectively.

Structure solutions and refinement of the structures were carried out using the SHELXTL-PLUS (5.03) software package (Sheldrick, G. M., Siemens Analytical X-ray Division, Madison, WI, 1997). The structures were solved by direct methods and refined successfully in the orthorhombic space group $P2_12_12_1$ for **3** and in the monoclinic space group $P2_1$ for **5**. Full matrix least-squares refinement was carried out by minimizing $\sum w(F_o^2 - F_c^2)^2$. The non-hydrogen atoms were refined anisotropically to convergence. The hydrogen atoms were treated using appropriate riding model (AFIX m3). Absolute structure was determined for both compounds (Flack $x = 0$ within experimental esd). The final residual values for the observed reflections [$I > 2\sigma(I)$], R(F), and wR(F^2) for all data and relevant structure refinement parameters are listed in Tables 1 and 5. The compound **3** crystallizes with a molecule of water as the solvent of crystallization. A projection view of the molecules with non-hydrogen atoms represented by 50% probability ellipsoids, and showing the atom labeling, is presented in Figures1 and 2 for complexes **3** and **5**, respectively.

For both complexes a list of atomic coordinates for the non-hydrogen atoms, complete listings of the geometrical parameters, positional and

Table 2. Bond Lengths [Å] for **3**

Mn(1)−N(1)	2.2984(11)	Mn(1)−N(3)	2.3060(13)
Mn(1)−N(4)	2.3330(12)	Mn(1)−N(2)	2.3470(12)
Mn(1)−N(5)	2.3492(11)	Mn(1)−C1(1)	2.6158(4)
Mn(1)−C1(2)	2.6563(4)	N(1)−C(5)	1.338(2)
N(1)−C(1)	1.345(2)	N(2)−C(6)	1.472(2)
N(2)−C(7)	1.480(2)	N(3)−C(13)	1.468(2)
N(3)−C(12)	1.476(2)	N(4)−C(14)	1.473(2)
N(4)−C(15)	1.475(2)	N(5)−C(21)	1.475(2)
N(5)−C(20)	1.483(2)	C(1)−C(2)	1.382(2)
C(1)−C(21)	1.519(2)	C(2)−C(3)	1.380(3)
C(3)−C(4)	1.378(3)	C(4)−C(5)	1.391(2)
C(5)−C(6)	1.517(2)	C(6)−C(22)	1.525(2)
C(7)−C(8)	1.527(2)	C(7)−C(12)	1.531(2)
C(8)−C(9)	1.529(2)	C(9)−C(10)	1.511(3)
C(10)−C(11)	1.517(3)	C(11)−C(12)	1.528(2)
C(13)−C(14)	1.514(2)	C(15)−C(20)	1.526(2)
C(15)−C(16)	1.532(2)	C(16)−C(17)	1.521(3)
C(17)−C(18)	1.503(4)	C(18)−C(19)	1.518(3)
C(19)−C(20)	1.531(2)	C(21)−C(23)	1.532(2)

Table 3. Bond Angles [deg] for **3**

N(1)−Mn(1)−N(3)	141.52(4)	N(1)−Mn(1)−N(4)	142.66(4)
N(3)−Mn(1)−N(4)	75.81(4)	N(1)−Mn(1)−N(2)	69.51(4)
N(3)−Mn(1)−N(2)	73.58(4)	N(4)−Mn(1)−N(2)	145.64(4)
N(1)−Mn(1)−N(5)	70.85(4)	N(3)−Mn(1)−N(5)	145.82(4)
N(4)−Mn(1)−N(5)	72.61(4)	N(2)−Mn(1)−N(5)	140.23(4)
N(1)−Mn(1)−C1(1)	91.40(3)	N(3)−Mn(1)−C1(1)	84.83(3)
N(4)−Mn(1)−C1(1)	91.84(4)	N(2)−Mn(1)−C1(1)	100.54(3)
N(5)−Mn(1)−C1(1)	83.45(3)	N(1)−Mn(1)−C1(2)	94.30(3)
N(3)−Mn(1)−C1(2)	89.22(3)	N(4)−Mn(1)−C1(2)	85.07(3)
N(2)−Mn(1)−C1(2)	79.30(3)	N(5)−Mn(1)−C1(2)	100.67(3)
C1(1)−Mn(1)−C1(2)	173.82(2)	C(5)−N(1)−C(1)	119.67(12)
C(5)−N(1)−Mn(1)	120.03(9)	C(1)−N(1)−Mn(1)	119.07(9)
C(6)−N(2)−C(7)	117.52(11)	C(6)−N(2)−Mn(1)	116.07(8)
C(7)−N(2)−Mn(1)	113.93(8)	C(13)−N(3)−C(12)	114.50(12)
C(13)−N(3)−Mn(1)	110.01(9)	C(12)−N(3)−Mn(1)	110.88(8)
C(14)−N(4)−C(15)	115.92(12)	C(14)−N(4)−Mn(1)	107.84(9)
C(15)−N(4)−Mn(1)	112.06(9)	C(21)−N(5)−C(20)	117.56(12)
C(21)−N(5)−Mn(1)	114.00(8)	C(20)−N(5)−Mn(1)	113.35(9)
N(1)−C(1)−C(2)	121.91(14)	N(1)−C(1)−C(21)	116.15(13)
C(2)−C(1)−C(21)	121.79(14)	C(3)−C(2)−C(1)	118.3(2)
C(4)−C(3)−C(2)	120.00(15)	C(3)−C(4)−C(5)	118.8(2)
N(1)−C(5)−C(4)	121.21(14)	N(1)−C(5)−C(6)	117.95(12)
C(4)−C(5)−C(6)	120.77(14)	N(2)−C(6)−C(5)	109.03(11)
N(2)−C(6)−C(22)	112.04(12)	C(5)−C(6)−C(22)	108.70(13)
N(2)−C(7)−C(8)	113.68(12)	N(2)−C(7)−C(12)	109.28(11)
C(8)−C(7)−C(12)	110.49(12)	C(7)−C(8)−C(9)	111.47(15)
C(10)−C(9)−C(8)	111.52(15)	C(9)−C(10)−C(11)	111.2(2)
C(10)−C(11)−C(12)	111.27(15)	N(3)−C(12)−C(11)	113.74(12)
N(3)−C(12)−C(7)	109.30(11)	C(11)−C(12)−C(7)	109.93(13)
N(3)−C(13)−C(14)	109.83(13)	N(4)−C(14)−C(13)	108.97(13)
N(4)−C(15)−C(20)	108.07(11)	N(4)−C(15)−C(16)	113.71(14)
C(20)−C(15)−C(16)	111.26(14)	C(17)−C(16)−C(15)	111.7(2)
C(18)−C(17)−C(16)	110.7(2)	C(17)−C(18)−C(19)	110.8(2)
C(18)−C(19)−C(20)	111.4(2)	N(5)−C(20)−C(15)	107.30(11)
N(5)−C(20)−C(19)	113.99(14)	C(15)−C(20)−C(19)	111.69(13)
N(5)−C(21)−C(1)	107.79(12)	N(5)−C(21)−C(23)	111.23(14)

(12) (a) Burkert, U.; Allinger, N. L. *Molecular Mechanics*; ACS Monograph 177; American Chemical Society: Washington, D. C., 1982. (b) Hancock, R. D. *Acc. Chem. Res.* **1990**, *23*, 253.
(13) Blessing, R. H. *Acta Crystallogr.* **1995**, *A51*, 33−38.

Table 4. Atomic Coordinates [$\times 10^{+4}$] and Equivalent Isotropic Displacement Parameters [$\Delta^2 \times 10^{+3}$] for **3**

	x	*y*	*z*	*U*(eq)[a]
Mn(1)	8079(1)	7748(1)	7900(1)	35(1)
C1(1)	10541(1)	7367(1)	7115(1)	57(1)
C1(2)	5631(1)	8299(1)	8653(1)	50(1)
O(1)	3087(2)	8722(1)	7460(1)	71(1)
N(1)	8376(1)	6608(1)	8586(1)	36(1)
N(2)	9324(1)	8058(1)	8993(1)	33(1)
N(3)	9007(2)	9049(1)	7794(1)	37(1)
N(4)	6730(2)	8262(1)	6907(1)	40(1)
N(5)	6896(2)	6656(1)	7304(1)	37(1)
C(1)	7748(2)	5911(1)	8352(1)	40(1)
C(2)	8164(2)	5178(1)	8647(1)	48(1)
C(3)	9205(2)	5173(1)	9219(1)	51(1)
C(4)	9816(2)	5887(1)	9476(1)	47(1)
C(5)	9404(2)	6601(1)	9133(1)	37(1)
C(6)	10174(2)	7392(1)	9346(1)	36(1)
C(7)	10077(2)	8863(1)	9008(1)	35(1)
C(8)	10198(2)	9226(1)	9759(1)	48(1)
C(9)	10958(2)	10062(1)	9742(1)	56(1)
C(10)	10096(3)	10617(1)	9230(1)	56(1)
C(11)	9982(2)	10252(1)	8486(1)	48(1)
C(12)	9170(2)	9430(1)	8506(1)	36(1)
C(13)	8023(2)	9501(1)	7284(1)	46(1)
C(14)	7609(2)	8972(1)	6648(1)	47(1)
C(15)	6399(2)	7635(1)	6366(1)	41(1)
C(16)	5296(3)	7915(1)	5761(1)	64(1)
C(17)	4893(3)	7232(2)	5249(1)	76(1)
C(18)	4159(2)	6538(2)	5647(1)	65(1)
C(19)	5270(2)	6232(1)	6228(1)	55(1)
C(20)	5720(2)	6902(1)	6754(1)	40(1)
C(21)	6468(2)	5981(1)	7781(1)	43(1)
C(22)	11920(2)	7366(1)	9133(1)	54(1)

[a] *U*(eq) is defined as one-third of the trace of the orthogonalized U_{ij} tensor.

Table 5. Crystal and Data and Structure Refinement for Complex **5**

empirical formula	$C_{23}H_{39}C1_2MnN_5$
fw	511.43
temp	223(2) K
wavelength	0.71073 Å
cryst syst	monoclinic
space group	$P2_1$
unit cell dimensions	$a = 12.1025(2)$ Å, $\alpha = 90°$ $b = 13.6848(2)$ Å, $\beta = 105.3870(10)°$ $c = 15.6309(2)$ Å, $\gamma = 90°$
V, *Z*	2496.00(6) Å^2, 4
D (calcd)	1.361 mg/m^3
absorption coefficient	0.763 mm^{-1}
F(000)	1084
cryst size	0.15 mm × 0.10 mm × 0.05 mm
∪ range for data collection	1.35−25.00°
limiting indices	$-15 < h \le 15$, $-18 \le k \le 18$, $0 \le 1 \le 21$
reflns collected	8771
independent reflns	8771 ($R_{int} = 0.0000$)
absorption correction	none
refinement method	full matrix least-squares on F^2
data/restraints/parameters	8723/1/559
goodness-of-fit on F^2	1.032
final R indices [$I > 2\sigma(I)$]	R1 = 0.0695, wR2 = 0.1036
R indices (all data)	R1 = 0.1517, wR2 = 0.1284
absolute structure parameter	−0.03(3)
largest diff peak and hole	0.407 and −0.340 eÅ^{-3}

isotropic displacement coefficients for hydrogen atoms, and anisotropic displacement coefficients for the non-hydrogen atoms are submitted as Supporting Information.

Syntheses. [Manganese(II)dichloro{2, 21-dimethyl-(4R,9R,14R,-19R)-3,10,13,20,26-pentaazatetracyclo [20.3.1.0^{4,9}.0^{14,19}]hexacosa-1(26),22(23),24-triene}], 2. A 500-mL round-bottom flask was charged with **1**[1,10] (10.0 g, 24.98 mmol) and 250 mL of anhydrous absolute ethanol. The white suspension was stirred under an Ar blanket while

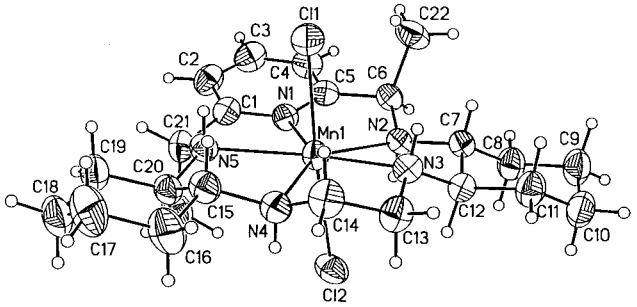

Figure 1. A projection view of **3** with non-hydrogen atoms represented by 50% thermal ellipsoids.

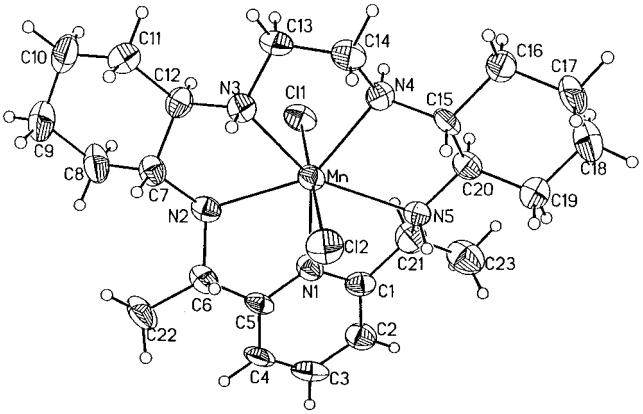

Figure 2. A projection view of the seven-coordinate molecule of **5** with non-hydrogen atoms represented by 50% thermal ellipsoids.

KOH (pellets, 6.35 g on the basis of 86.9% material, 4 equiv, 0.1 mol) was added in one portion. The suspension was warmed slightly to 30 °C and stirring continued for an additional hour until all the solids had dissolved. At that point $MnCl_2$ (anhydrous, 3.15 g, 24.99 mmol) was added under dry Ar in one portion to the fine white suspension. The color turned green-gray, then gray. One hour later, when all the $MnCl_2$ had dissolved, 2,6-diacetylpyridine (4.08 g, 24.97 mmol) was added as a solid in one portion. The suspension was stirred at room temperature for 30 min, then heated to reflux. The suspension acquired a yellowish coloration once reflux was attained. After refluxing for 96 h, the deep red-orange suspension was allowed to cool to room temperature over the course of 2 h. Suspended solids were filtered using a 10 μm fritted funnel and washed with cold absolute EtOH (0 °C, 2 × 50 mL). The filtrate was removed using a rotary evaporator, and the remaining red-orange residue was allowed to dry in vacuo overnight (room temperature, 0.3 Torr). The next day, 13.55 g (107% crude yield) of an amorphous red-orange solid remained. HPLC indicated 94% product ($t_R = 3.23$ min using 10−50% gradient). The crude material may be purified to 98% purity by extractive workup as follows: 40 g of the crude material isolated after drying in vacuo is dissolved in 800 mL of distilled water and extracted with CH_2Cl_2 (2 × 500 mL). The light orange organic layer was separated. Then, 160 g of NaCl was added to the aqueous layer (ca. 20% in NaCl) and extracted with CH_2Cl_2 (2 × 500 mL). Upon separating and pooling the organic layers, drying over $MgSO_4$ (10 g for 5 min with stirring), and filtering through a 10 μm fritted funnel, the solvent was removed in a rotary evaporator (water bath temperature ≤35 °C). After drying in vacuo overnight (room temperature, 0.3 Torr), 34 g of purified bis-imine (85% recovery) was isolated as an orange amorphous powder ≥98% by HPLC. MS (ESI) $m/z = 471$ [M-Cl]$^+$.

[Manganese(II)dichloro{2*R*, 21*R*-dimethyl-(4R,9R,14R,19R)-3,-10,13,20,26-pentaazatetracyclo [20.3.1.0^{4,9}.0^{14,19}]hexacosa-1(26),22-(23),24-triene}] (3). Bisimine complex **2** (2.0 g, 3.94 mmol) was dissolved in 40 mL of anhydrous EtOH, and the flask was flushed with Ar for a few minutes. $NaBH_4$ (1.2 g, 31.5 mmol, ca. 4 equiv/double bond) was added to the orange solution in one portion, and the suspension was stirred at room temperature. After 2 h, the temperature was increased to 50 °C and heated for 5 h, then cooled to ambient and

the solvent was removed from the pale yellow mixture. The residue was stirred with 0.5 M LiCl in MeOH (100 mL) until effervescence subsided (~ 1 h). After removing MeOH, water (150 mL) was added to the residue, and it was stirred until all solids dissolved. NaCl (45 g) was added, and, once dissolved, the aqueous solution was extracted with CH_2Cl_2 (3 × 100 mL). The combined organic extracts were dried ($MgSO_4$) and filtered, and the solvent was evaporated to dryness. The crude solid, complex **3**, was 96% pure by HPLC and was purified by SiO_2 flash chromatography (20 g SiO_2 per 1 g of crude **3**) using 5% MeOH/CH_2Cl_2 as eluant. Upon drying in vacuo (50 °C, 0.5 Torr, 18 h), complex **3** was isolated as an off-white solid (1.87 g, 93% yield) with a purity ≥98% by HPLC. MS (ESI) m/z = 261 [M − 2Cl + $2CH_3CN$]$^{2+}$; MS (LRFAB) m/z = 475 [M-Cl]$^+$. Anal. Calcd for $C_{23}H_{39}Cl_2N_5Mn$: C, 54.01; H, 7.69; Cl, 13.86; N, 13.69. Found: C, 53.65; H, 7.61; Cl, 13.11; N, 12.90.

Crystals of complex **3** suitable for X-ray structure determination were obtained by crystallizing approximately 30 mg of **3** from 2 mL of 1:1 THF/Et_2O.

To characterize via NMR the ligand coordinated to the paramagnetic high-spin d^5 metal Mn(II), the ligand was removed from the metal via the following procedure.

Synthesis of *R,R*-Dimethyl Ligand of Complex 3, 4. To a stirred solution containing the complex **3** prepared above (5.11 g, 10.0 mmol) in 50 mL H_2O was added a solution of Na_2S·9 H_2O (4.80 g, (20.0 mmol)) in 10 mL H_2O dropwise. A precipitate formed as the solution was stirred at room temperature. At 3 h, the mixture was warmed to 60 °C, and the stirring continued for an additional 75 h. At this point mass spectral analysis indicated that little complex remained. The mixture was then stirred with warming for 8 h, allowed to stand for 60 h, and was filtered. The solids were washed with MeOH (100 mL), and the filtrate was concentrated to a volume of 20 mL. THF (250 mL) was then added, and the solution was concentrated to 50 mL. The solution was taken to dryness and then redissolved in THF and filtered. To the filtrate was added 300 mL diethyl ether. After allowing to stand overnight, the solids were filtered off and washed with ethyl ether. The filtrate was reduced to dryness and MeOH (5 mL) was added. A rapid crystallization occurred, and additional MeOH (10 mL) was added to dissolve the solid and the solution was concentrated to the point of crystallization. Adding ethyl ether resulted in a very crystalline pink solid. The solid was removed via filtration, and was washed with diethyl ether (2 × 100 mL). The filtrate was reduced to dryness, dried, and afforded 2.75 g of solid ligand, confirmed by MS, HPLC, and ^{1}H NMR analysis. The solid was dissolved in MeCN (5 mL)/H_2O (10 mL), and TFA (2 mL) was added, resulting in the formation of an off-white crystalline solid. This isomer readily crystallized from H_2O. The product was crystallized from H_2O to give a total of three crops (2.12 g) of the tris·TFA salt which ranged from 93.6% to 98.8% in purity via HPLC. The three crops were combined and dissolved in hot H_2O (20 mL). Upon allowing the solution to slowly cool to room temperature, a large cluster of 1 cm × 2 mm × 1 mm crystals formed. The solvent was removed from these crystals via decantation, and the crystals were washed with H_2O (2 mL). Upon drying in vacuo, the needles disintegrated to give 1.07 g of the product as a white powder. A second crop of 540 mg was obtained for a total of 1.61 g (22.1% yield); HPLC (Vydac 218TP54 protein and peptide C18 (100:0 to 75:25 H_2O with 0.1% TFA/CH_3CN gradient over 15 min; flow = 1 mL/min; 10 μL inj vol.)); 100%; t_R = 11.89 min.

To a stirred solution of this ligand, tris·TFA salt (1.49 g, 2.05 mmol), in anhydrous MeOH (30 mL) was added KOH (0.529 g-87%, 8.19 mmol). Upon dissolution of the KOH, the solvent was removed in vacuo and the remaining H_2O was removed via azeotropic distillation with EtOH (60 mL). The resulting foam was crushed, ethyl ether (30 mL) was added, and the mixture was filtered. The off-white powder was washed with ethyl ether (2 × 25 mL), the combined filtrate and washings were combined, and the solvent was removed in vacuo to give 880 mg of the crude product as a pale yellow solid. The solid was dissolved in hexanes (20 mL) and filtered through a 1 μM PTFE filter to remove a very small amount of solid. The solvent was removed in vacuo, and the resulting glass was dissolved in ethyl ether (1 mL). Removal of the solvent and drying of the resulting foam in vacuo gave 810 mg (quantitative yield of the pure *R,R*-dimethyl ligand, **4**: ^{1}H NMR (C_6D_6, 300 MHz) δ 7.09 (t, J = 7.7 Hz, 1 H), 6.67 (d, J = 7.7 Hz, 2 H), 4.23 (br m, 2 H), 3.60 (m, 2 H), 3.03 (m, 2 H), 2.62 (m, 2 H), 2.45 (m, 2 H), 2.31 (m, 2 H), 2.10 (m, 4 H), 1.67 (m, 4 H), 1.42 (br s, 2 H), 1.25 (d, J = 6.44 Hz, 6 H), 1.11 (m, 8 H); ^{13}C NMR (C_6D_6, 75 MHz) δ 163.78, 136.15, 118.87, 62.85, 56.81, 53.05, 47.91, 31.81, 25.43, 25.07, 21.60; LR MS (CI−CH_4) m/z 386 [M + H] $^+$; HR MS (ESI) 386.3323 [M + H]$^+$ (386.3284 calcd for $C_{23}H_{39}N_5$); HPLC (Vydac 218TP54 protein and peptide C18 (100:0 to 80:20 H_2O with 0.1% TFA/CH_3CN gradient over 40 min; flow = 1 mL/min; 5 μL inj. vol); 99.0% purity with a 99.8:0.2% ratio for *R,R* to *R,S* dimethyl isomers, t_R = 12.75 and 12.56 min, respectively.

[Manganese(II)dichloro{2*S*, 21*S*-dimethyl-(4R,9R,14R,19R)-3,-10,13,20,26-pentaazatetracyclo [20.3.1.0^{4,9}0^{14,19}]hexacosa-1(26),22-(23),24-triene}], 5. Bisimine **2** (15.0 g, 29.6 mmol) was dissolved in 1.5 L of anhydrous MeOH, and the flask was flushed with Ar for a few minutes. Pd/C (3 wt % Pd, 7.5 g, 50% by wt) was carefully added under a blanket of Ar. As the black suspension was heated (ca. 45 °C), solid ammonium formate (7.5 g, 118.9 mmol, 2 equiv/double bond) was added. One hour after reflux was attained, HPLC indicated the absence of diimine, **2**, and 35% and 65% of monoimine intermediate in combination with the desired product **5** and *R,S*-diastereomer **6** (relative ratio ca. 3.5:1), respectively. A second portion of formate (3.75 g, 59.5 mmol, 1 equiv/double bond) was added, and the suspension was stirred/refluxed for an additional 1.5 h. The black suspension was allowed to cool to ambient temperature and was filtered through a 5 cm bed of alumina (Al_2O_3, Brockmann grade, neutral, previously washed with MeOH). The bed of catalyst and alumina was washed with MeOH (2 × 100 mL), and the combined solvents were removed under reduced pressure to yield light yellow foam (14.7 g).

Purification by RPS C18 Chromatography. Bakerbond Octadecyl C_{18} (160 g) was packed into a 50 mm × 140 mm glass column. The column was equilibrated with CH_3CN (500 mL), followed by 0.5 M aq NaCl/CH_3CN (1:1, 500 mL), and finally with 18% CH_3CN in 0.25M aq NaCl (500 mL). The crude foam containing a mixture of diastereomers **5** and **6** (6 g) was dissolved in 15 mL water, the pH was adjusted to 7.5 with 1% aq NaOH, and the solution was loaded atop the column. The product was eluted isocratically with 18% CH_3CN in 0.5 M aq NaCl at an approximate flow rate of 1 drop per second. Fractions with HPLC purities =96% were combined and concentrated to about 300 mL under reduced pressure. Sodium chloride (8.8 g) was added to adjust the concentration to ca. 1.0 M, and the aqueous solution was extracted with CH_2Cl_2 (300 and 150 mL). After drying over Na_2SO_4, CH_2Cl_2 was evaporated to dryness to yield off-white foam. The foam was stirred in absolute ethanol (10 mL) for 15 min, filtered through a bed of EtOH-washed Celite and the solvent was removed to dryness and finally dried in vacuo (0.5 Torr, 50 °C, 18 h) to afford 3.85 g (64% yield based on **2**) of *S,S*-isomer **5** with a purity ≥98% by HPLC. MS (ESI) m/z = 475 [M − Cl]$^+$. Analysis calcd for $C_{23}H_{39}C_{l2}N_5Mn$: C, 54.01; H, 7.69; Cl, 13.86; N, 13.86. Found: C, 53.79; H, 7.69; Cl, 13.86; N 13.69.

Crystals of complex **5** suitable for X-ray structure determination were obtained by crystallization of **5** from a 1:1:1 THF/MTBE/MeOH solvent mixture.

Synthesis of *S,S*-Dimethyl Ligand of Complex 5, 7. This *S,S*-dimethyl substituted ligand was synthesized in a manner identical to that outlined above for ligand **4** using the sulfide formation chemistry for removal of the metal from the macrocyclic ligand. ^{1}H NMR (C_6D_6, 300 MHz) δ 7.15 (d, J = 7.6 Hz, 1 H), 6.75 (d, J = 7.7 Hz, 2 H), 3.98 (br m, 2 H), 3.07 (m, 2 H), 2.84 (m, 2 H), 2.46 (m, 2 H), 2.22 (m, 4 H), 2.15 (m, 2 H), 1.91 (m, 4 H), 1.60 (m, 4 H), 1.47 (d, J = 6.6 Hz, 6 H), 1.1 (m, 6 H), 0.9 (m, 2 H); ^{13}C NMR (C_6D_6, 75 MHz) δ 164.80, 135.92, 119.09, 61.89, 61.38, 57.58, 46.87, 33.81, 32.58, 25.54, 25.18, 23.79; LR MS (CI−CH_4) m/z 386 [M + H] $^+$; HR MS (ESI) 386.3323 [M + H]$^+$ (386.3284 calcd for $C_{23}H_{39}N_5$).

[Manganese(II)dichloro{2*R*, 21*S*-dimethyl-(4R,9R,14R,19R)-3,-10,13,20,26-pentaazatetracyclo [20.3.1.0^{4,9}.0^{14,19}]hexacosa-1(26),22-(23),24-triene}], 6. Complex **6** was obtained as a byproduct during the synthesis of the *S,S*-isomer **5.** Complex **6** was isolated in 23% yield, in a way analogous to **5**, from selected fractions obtained during the purification of the latter. Purity was 97% by HPLC. MS (ESI): m/z 475 [M − Cl]$^+$.

Synthesis of *R,S*-Dimethyl Ligand of Complex 6, 8. The *R,S*-dimethyl substituted ligand was synthesized in a manner identical to that outlined above for ligand **4** using the sulfide formation chemistry for removal of the metal from the macrocyclic ligand. ^{1}H NMR ($CDCl_3$, 300 MHz) δ 7.5 (quartet, $J = 7.6$ Hz, 1 H), 6.99 (d, $J = 7.7$ Hz, 2 H), 4.24 (quartet, $J = 6.5$ Hz, 2 H), 3.44 (s, 2 H), 2.90 (d, $J = 6.6$ Hz, 2 H), 2.60 (m, 4 H), 2.38 (m, 6 H), 2.10 (m, 4 H), 1.75 (d, $J = 8.7$ Hz, 2 H), 1.27 (d, $J = 6.4$ Hz, 6 H), 1.22 (s, 2 H), 1.17 (m, 6 H); ^{13}C NMR ($CDCl_3$, 75 MHz) δ 162.51, 136.40, 119.49, 113.39, 64.16, 62.47, 56.06, 55.30, 52.29, 47.16, 35.99, 31.64, 30.89, 29.45, 25.35, 25.29, 25.13, 24.65, 21.80d; LR MS (CI−CH_4) *m/z* 386 $[M + H]^+$; HR MS (ESI) 386.3323 $[M + H]^+$ (386.3284 calcd for $C_{23}H_{39}N_5$).

Results

Synthesis and Characterization. The template reaction producing the bisimine complex **2** can be carried out in high yield using a modification of the method of refs 1, 8, and 9. The reduction/conversion of this complex to the three diastereomers, **3**, **5**, and **6**, with high diastereomeric purity is an obvious problem. When the borohydride conditions utilized for synthesis of the complex M40403 were utilized for the reduction of the dimethyl substituted bisimine, **2**, we found that only one isomer is produced during the reduction as monitored by HPLC. This borohydride route produces the *R,R*-diastereomer as confirmed by single-crystal X-ray structure analysis as reported here. This result is perhaps not surprising when one inspects models of the precursor complex **2**. The least stereochemically restricted direction of approach to the imine double bond will be from the opposite side of the macrocyclic ring plane from the axial CH of the cyclohexyl ring carbon adjacent to the imine double bond carbon. This approach yields the *R,R*-diastereomer.

On the basis of this analysis, the other isomers are clearly less likely to be produced using a homogeneous catalyst; thus, heterogeneous catalysts offered the best possibility that *S*-centers could be generated when the complex is adsorbed onto a surface with surface hydrides bound. The best catalyst combination we found for producing the desired *S*-centers is use of Pd on charcoal with ammonium formate as a hydrogen source, i.e., transfer hydrogenation with the heterogeneous Pd catalyst. Under the conditions described in the Experimental Section, the chemical yields of the *S,S* + *S,R* diastereomers **5** and **6** were over 99% and the ratio of yields (*S,S*/*S,R*) could be achieved with over 3:1 selectivity.

To characterize these unique diastereomeric ligands by NMR spectroscopy, it was necessary to remove the highly paramagnetic high-spin d^5 Mn(II) ion from the complex. This was achieved using sulfide ion induced Mn sulfide precipitation. The high inherent stability of the complexes is demonstrated with this process as the removal of the metal is a very slow process. In any event, each of the three diastereomeric ligands possesses a unique ^{1}H NMR and ^{13}C NMR spectra.

Crystal Structure of Complexes 3 and 5. The dichloro Mn(II) complex, **3**, crystallizes in an orthorhombic space group $P2_12_12_1$ (see Table 1 for details) with one molecule of water per molecule of complex in the unit cell hydrogen-bonded to the bound chloride ligands. A projection view of the molecule with non-hydrogen atoms represented by 50% thermal ellipsoids is shown in Figure 1, and selected bond lengths (Table 2), bond angles (Table 3), and atom coordinates (Table 4) are listed. The Mn(II) complex exists in the *trans*-dichloro seven-coordinate geometry, the common structure which we have observed for this general class of [Mn([15]aneN$_5$)Cl$_2$] complexes.[2,3,8,14] The Mn(II) and the nitrogen atoms of the macrocycle are coplanar; thus, the coordination sphere is best described as pentagonal bipyramidal. The metal-nitrogen bond distances range from 2.29 to 2.34 Å with the Mn−N avg bond distance being 2.323 Å and the Mn−Cl distances are approximately 2.66 Å and 2.62 Å. The Cl−Mn−Cl angle is approximately 174° as it appears that the chlorines are repelled by the diaxial methyl group conformations. The sum of the five N−Mn−N chelate angles add up to 362.36°(with an average of 72.47°), very close to 360°for an ideal planar structure. The observed diaxial methyl disposition is unexpected, but does satisfy the conformational constraint that the C−CH_3 and NH pattern about the macrocycle is alternating up−down-up−down. The actual stereochemistry of the carbon centers bearing the methyl substituents is *R*. It is worthwhile to compare this structure with those of other [Mn(II)([15]aneN$_5$)Cl$_2$] complexes in this series for which we have obtained crystallographic data. For example, previous complexes, including one in which a fused pyridino moiety was present,[3] possessed the Mn−N avg. bond distance of 2.31 Å and Mn−Cl avg. distances of 2.56 Å and 2.63 Å- -values which are quite similar to those obtained for this complex **3**.

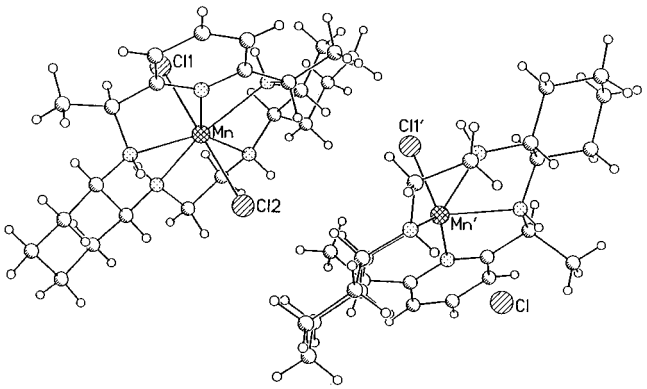

Figure 3. The unit cell containing the two different molecules of **5**.

The dichloro Mn(II) complex, **5**, crystallizes in a monoclinic space group $P2_1$ (see Table 5 for details) with two distinctly different molecules of complex in the unit cell. One form of the complex possesses the trans-dichloro seven-coordinate geometry observed with complex **3**, but the second molecule possesses a very different ligand conformation about the Mn(II) producing a six-coordinate ligand environment with a nonbonded or ionic chloride. In Figure 2 a projection view of the seven-coordinate molecule of **5** with non-hydrogen atoms represented by 50% thermal ellipsoids is shown, and in Figure 3 the two different molecules of **5** that occupy the unit cell are shown. In Table 6 selected bond lengths are presented, in Table 7 selected bond angles are presented, and in Table 8 atom coordinates are listed.

Several features of this structure determination are of interest. For both crystalmorphs of complex **5** the methyl groups are in the *S* absolute configuration; thus, the two different conformations of complex **5** observed in the unit cell (one of which produces a noncoordinated chloride ion) are not due to stereoisomer differences. The structure of the seven-coordinate form is similar to that of **3**, but the methyl groups are now equatorial for this *S,S*-isomer, not the diaxial orientation observed with the *R,R*-isomer **3**. For the seven-coordinate form of complex **5** the five Mn−N bond lengths are 2.238, 2.308, 2.412, 2.297, and 2.354 Å affording an avg. Mn−N bond distance of 2.322 Å, ca. 2.323 Å for **3**. Of special interest are the Mn−Cl distances

(14) Neumann, W. L.; Franklin, G.; Sample, K.; Aston, K.; Weiss, R.; Riley, D. P. *Tetrahedron Lett.* **1997**, *38*(5), 779.

Table 6. Bond Lengths [Å] for **5**

Mn−N(1)	2.238(6)	Mn−N(4)	2.297(6)
Mn−N(3)	2.308(5)	Mn−N(2)	2.354(6)
Mn−N(5)	2.412(6)	Mn−C1(1)	2.589(2)
Mn−C1(2)	2.597(2)	Mn′−N(1′)	2.219(6)
Mn′−N(3′)	2.259(6)	Mn′−N(5′)	2.304(6)
Mn′−N(4′)	2.361(6)	Mn′−N(2′)	2.362(6)
Mn′−C1(1′)	2.464(2)	N(1)−C(5)	1.341(8)
N(1)−C(1)	1.369(8)	N(2)−C(7)	1.486(8)
N(2)−C(6)	1.489(8)	N(3)−C(12)	1.468(8)
N(3)−C(13)	1.469(8)	N(4)−C(15)	1.463(8)
N(4)−C(14)	1.471(8)	N(5)−C(20)	1.471(8)
N(5)−C(21)	1.477(9)	N(1′)−C(1′)	1.333(8)
N(1′)−C(5′)	1.335(9)	N(2′)−C(20′)	1.465(8)
N(2′)−C(21′)	1.466(8)	N(3′)−C(15′)	1.477(8)
N(3′)−C(14′)	1.480(8)	N(4′)−C(13′)	1.461(8)
N(4′)−C(12′)	1.465(8)	N(5′)−C(7′)	1.470(8)
N(5′)−C(6′)	1.478(8)	C(1)−C(2)	1.379(9)
C(1)−C(21)	1.525(10)	C(2)−C(3)	1.388(11)
C(3)−C(4)	1.362(10)	C(4)−C(5)	1.387(9)
C(5)−C(6)	1.525(9)	C(6)−C(22)	1.509(10)
C(7)−C(8)	1.514(9)	C(7)−C(12)	1.544(9)
C(8)−C(9)	1.522(10)	C(9)−C(10)	1.512(10)
C(10)−C(11)	1.525(10)	C(11)−C(12)	1.515(9)
C(13)−C(14)	1.490(9)	C(15)−C(16)	1.535(9)
C(15)−C(20)	1.550(9)	C(16)−C(17)	1.524(9)
C(17)−C(18)	1.501(10)	C(18)−C(19)	1.531(10)
C(19)−C(20)	1.518(10)	C(21)−C(23)	1.486(10)
C(1′)−C(2′)	1.396(9)	C(1′)−C(21′)	1.527(10)
C(2′)−C(3′)	1.365(10)	C(3′)−C(4′)	1.373(10)
C(4′)−C(5′)	1.392(9)	C(5′)−C(6′)	1.508(10)
C(6′)−C(22′)	1.539(9)	C(7′)−C(12′)	1.535(9)
C(7′)−C(8′)	1.541(9)	C(8′)−C(9′)	1.528(10)
C(9′)−C(10′)	1.518(10)	C(10′)−C(11′)	1.549(10)
C(11′)−C(12′)	1.543(9)	C(13′)−C(14′)	1.513(9)
C(15′)−C(20′)	1.516(9)	C(15′)−C(16′)	1.531(9)
C(16′)−C(17′)	1.521(11)	C(17′)−C(18′)	1.533(10)
C(18′)−C(19′)	1.492(9)	C(19′)−C(20′)	1.525(10)
C(21′)−C(23′)	1.538(10)		

that are 2.589 Å and 2.597 Å, which are within the range observed previously for complexes in this class. The sum of the five N−Mn−N chelate angles add up to 361.40°(with an average of 72.28°), very close to 360°for an ideal planar structure and even closer to planarity than observed with **3**.

The most remarkable aspect of this structure determination is the observation that a second structurally unique molecule of **5** is present in the unit cell with a nonbonded chloride; i.e., the Mn to chlorine distances are 2.464 and 3.115 Å. The coordinated chlorine actually has a shorter Mn−Cl bond distance than that of the other complexes we have observed in this class: nearly 0.1 Å., while the non bonded chlorine is nearly 0.5−0.6 Å further from the metal than observed with these complexes. The Mn−N bond distances range from 2.219 to 2.362 Å with a Mn−N bond distance average of 2.301 Å—approximately 0.02 Å shorter than observed for the 7-coordinate crystalmorph. More striking is the degree of nonplanarity of the ligand about the Mn(II), i.e., the degree of folding. The sum of the five N−Mn−N chelate ring angles is 367.2° for this six-coordinate form of **5** and the five bond angles Cl−Mn−N are 84.68°, 93.2°, 97.0°, 93.6°, and 120.3°. Thus, the structure shows that N_3 is folded well below the plane defined by the Mn and the nitrogen atoms of the remaining three secondary amine donors and the pyridine. This six-coordinate complex also has a different conformation of the dimethyl substituents; i.e., they are *diaxial S,S*-dimethyl substituted, while ligand still retains the conformational constraint that the CH and NH pattern about the macrocycle is alternating up−down−up−down. Thus, this *S,S*-dimethyl substituted ligand possesses a driving force for folding of the ligand so as to adopt a six-coordinate pseudooctahedral geometry about the spherically symmetrical Mn(II) ion, which is sufficient to overcome the Coulombic attractive force of binding the chloride ion to the positive Mn center.

Catalytic Activity and Stability of Complexes 3, 5, and 6. The catalytic activities of each of the three new complexes were measured as function of pH and are listed in Table 9 along with the unsubstituted complex, M40403, for comparison. The *meso* (or *cis-R,S*) complex **6** exhibits a catalytic SOD rate approximately the same as that of the unsubstituted complex M40403. In contrast, the *R,R*-dimethyl substituted complex, **3**, has no measurable rate for dismutation of superoxide, while the other *trans* isomer, the *S,S*-dimethyl complex, **5**, exhibits a very fast rate constant for SOD catalysis. This rate is about 2 orders of magnitude greater than that of the parent unsubstituted complex, M40403, and actually exceeds that of the native Mn SOD enzyme. This dramatic improvement in rate is associated with some loss in kinetic stability of the complex compared to M40403, but the complex is nevertheless very stable in aqueous media such that at pH 7 it is stable indefinitely, even in the presence of added chelator ligands such as EDTA. The kinetics for dissociation of the ligand from the metal are first-order in [complex] and first-order in [H+]. The second-order rate constant in Table 9 (k_{diss}) allows one to calculate the half-life for dissociation at any pH by first calculating the first-order rate constant at the pH of interest by multiplying the listed second-order rate constant, k_{diss}, by the [H+]. Thus, at pH = 5.5 (the pH of ischemic tissue), the rate constant for proton assisted dissociation of the complex is 3.2×10^{-6} s^{-1}; consequently, the half-life for dissociation is approximately 60 h. This high level of inherent chemical stability is reflected in preliminary metabolism studies which show that in rodents this complex is completely stable in blood, tissue and organs and is excreted intact.

Molecular Mechanics (MM) Studies. Our previously reported mechanistic studies reveal that the rate-determining step in the catalytic cycle for superoxide dismutation with this family of [Mn(II)([15]aneN_5)X_2] involves oxidation of a Mn(II) center to Mn(III). There are two pathways to accomplish this: (1) a pH independent inner-sphere binding of superoxide to a vacant coordination site on the Mn(II)—a process which is rate-limiting based on the rate of formation of a vacant axial coordination site, and (2) a pH dependent process which involves a proton-coupled electron transfer (H atom transfer) from a water bound on Mn(II) to an incoming $HO_2^{\cdot}$.[2,8] This process accounts for most of the catalytic activity at pH ≤ 7.4 for these complexes and would be expected to be maximally efficient when the structure of the reduced Mn(II) complex resembles that of the oxidized product,[15] i.e., when the Mn(II) complex adopts a folded ligand geometry approaching a six-coordinate pseudooctahedral geometry. Thus, folding of an amine donor in the fifteen-membered macrocyclic ring ligand so that it occupies an axial site would generate a pseudooctahedral complex. If the ligand contains substituents which, due to intramolecular steric repulsions and angle strains, could force this folded pseudooctahedral geometry about the spherically symmetrical Mn(II) ion, then the Mn(II) complex would be poised to undergo facile electron transfer as the ligand reorganization energy barrier would be lowered. Thus, a good catalyst will then be one in which the Mn(II) center is constrained in a geometry that promotes fast electron-transfer, i.e., a pseudooctahedral geometry preferred by Mn(III).

As described previously,[2] the modeling paradigm we have successfully employed to correlate rate constants for the catalytic

(15) Marcus, R. A. *Annu. Rev. Phys. Chem.* **1964**, *15*, 155.

Table 7. Bond Angles [deg] for **5**[a]

N(1)−Mn−N(4)	142.7(2)	N(1)−Mn−N(3)	140.8(2)	C(4)−C(3)−C(2)	121.5(7)	C(3)−C(4)−C(5)	118.7(7)
N(4)−Mn−N(3)	76.4(2)	N(1)−Mn−N(2)	69.2(2)	N(1)−C(5)−C(4)	120.7(7)	N(1)−C(5)−C(6)	113.7(6)
N(4)−Mn−N(2)	147.5(2)	N(3)−Mn−N(2)	72.9(2)	C(4)−C(5)−C(6)	125.6(7)	N(2)−C(6)−C(22)	118.7(6)
N(1)−Mn−N(5)	69.7(2)	N(4)−Mn−N(5)	73.2(2)	N(2)−C(6)−C(5)	105.6(5)	C(22)−C(6)−C(5)	114.1(6)
N(3)−Mn−N(5)	147.4(2)	N(2)−Mn−N(5)	138.8(2)	N(2)−C(7)−C(8)	114.1(6)	N(2)−C(7)−C(12)	108.1(6)
N(1)−Mn−C1(1)	91.2(2)	N(4)−Mn−C1(1)	88.1(2)	C(8)−C(7)−C(12)	109.4(6)	C(7)−C(8)−C(9)	112.0(6)
N(3)−Mn−C1(1)	95.0(2)	N(2)−Mn−C1(1)	84.26(14)	C(10)−C(9)−C(8)	112.0(7)	C(9)−C(10)−C(11)	110.2(6)
N(5)−Mn−C1(1)	95.46(14)	N(1)−Mn−C1(2)	88.6(2)	C(12)−C(11)−C(10)	112.7(6)	N(3)−C(12)−C(11)	114.9(6)
N(4)−Mn−C1(2)	91.8(2)	N(3)−Mn−C1(2)	85.5(2)	N(3)−C(12)−C(7)	109.8(6)	C(11)−C(12)−C(7)	109.6(6)
N(2)−Mn−C1(2)	96.11(14)	N(5)−Mn−C1(2)	84.00(14)	N(3)−C(13)−C(14)	110.1(6)	N(4)−C(14)−C(13)	110.8(6)
C1(1)−Mn−C1(2)	179.46(8)	N(1′)−Mn′−N(3′)	133.7(2)	N(4)−C(15)−C(16)	114.0(6)	N(4)−C(15)−C(20)	109.7(5)
N(1′)−Mn′−N(5′)	74.1(2)	N(3′)−Mn′−N(5′)	125.9(2)	C(16)−C(15)−C(20)	109.6(6)	C(17)−C(16)−C(15)	112.5(6)
N(1′)−Mn′−N(4′)	146.0(2)	N(3′)−Mn′−N(4′)	73.6(2)	C(18)−C(17)−C(16)	109.2(7)	C(17)−C(18)−C(19)	111.6(7)
N(5′)−Mn′−N(4′)	72.6(2)	N(1′)−Mn′−N(2′)	73.7(2)	C(20)−C(19)−C(18)	112.6(6)	N(5)−C(20)−C(19)	113.3(6)
N(3′)−Mn′−N(2′)	73.2(2)	N(5′)−Mn′−N(2′)	146.6(2)	N(5)−C(20)−C(15)	108.8(5)	C(19)−C(20)−C(15)	108.2(6)
N(4′)−Mn′−N(2′)	140.2(2)	N(1′)−Mn′−C1(1′)	93.2(2)	N(5)−C(21)−C(23)	119.4(7)	N(5)−C(21)−C(1)	106.1(6)
N(3′)−Mn′−C1(1′)	120.3(2)	N(5′)−Mn′−C1(1′)	97.0(2)	C(23)−C(21)−C(1)	113.9(6)	N(1′)−C(1′)−C(2′)	121.0(7)
N(4′)−Mn′−C1(1′)	84.68(14)	N(2′)−Mn′−C1(1′)	93.6(2)	N(1′)−C(1′)−C(21′)	119.8(6)	C(2′)−C(1′)−C(21′)	119.1(7)
C(5)−N(1)−C(1)	120.8(6)	C(5)−N(1)−Mn	119.8(5)	C(3′)−C(2′)−C(1′)	117.9(8)	C(2′)−C(3′)−C(4′)	120.8(7)
C(1)−N(1)−Mn	119.4(5)	C(7)−N(2)−C(6)	116.6(5)	C(3′)−C(4′)−C(5′)	119.0(8)	N(1′)−C(5′)−C(4′)	119.9(7)
C(7)−N(2)−Mn	115.2(4)	C(6)−N(2)−Mn	106.1(4)	N(1′)−C(5′)−C(6′)	119.1(6)	C(4′)−C(5′)−C(6′)	121.1(7)
C(12)−N(3)−C(13)	115.0(5)	C(12)−N(3)−Mn	109.9(4)	N(5′)−C(6′)−C(5′)	112.3(6)	N(5′)−C(6′)−C(22′)	111.3(6)
C(13)−N(3)−Mn	109.2(4)	C(15)−N(4)−C(14)	115.5(5)	C(5′)−C(6′)−C(22′)	109.6(6)	N(5′)−C(7′)−C(12′)	107.2(6)
C(15)−N(4)−Mn	111.7(4)	C(14)−N(4)−Mn	108.6(4)	N(5′)−C(7′)−C(8′)	116.1(6)	C(12′)−C(7′)−C(8′)	109.5(6)
C(20)−N(5)−C(21)	118.9(6)	C(20)−N(5)−Mn	112.4(4)	C(9′)−C(8′)−C(7′)	110.3(6)	C(10′)−C(9′)−C(8′)	112.1(7)
C(21)−N(5)−Mn	104.6(4)	C(1′)−N(1′)−C(5′)	121.4(6)	C(9′)−C(10′)−C(11′)	109.5(7)	C(12′)−C(11′)−C(10′)	112.9(7)
C(1′)−N(1′)−Mn′	119.2(5)	C(5′)−N(1′)−Mn′	118.9(5)	N(4′)−C(12′)−C(7′)	110.3(6)	N(4′)−C(12′)−C(11′)	112.7(6)
C(20′)−N(2′)−C(21′)	116.9(6)	C(20′)−N(2′)−Mn′	106.4(4)	C(7′)−C(12′)−C(11′)	111.5(6)	N(4′)−C(13′)−C(14′)	108.4(6)
C(21′)−N(2′)−Mn′	113.2(4)	C(15′)−N(3′)−C(14′)	116.9(5)	N(3′)−C(14′)−C(13′)	109.0(6)	N(3′)−C(15′)−C(20′)	108.5(5)
C(15′)−N(3′)−Mn′	115.5(4)	C(14′)−N(3′)−Mn′	112.1(4)	N(3′)−C(15′)−C(16′)	112.1(6)	C(20′)−C(15′)−C(16′)	112.5(6)
C(13′)−N(4′)−C(12′)	114.8(6)	C(13′)−N(4′)−Mn′	112.5(4)	C(17′)−C(16′)−C(15′)	111.8(6)	C(16′)−C(17′)−C(18′)	110.0(6)
C(12′)−N(4′)−Mn′	113.7(4)	C(7′)−N(5′)−C(6′)	115.8(6)	C(19′)−C(18′)−C(17′)	110.6(6)	C(18′)−C(19′)−C(20′)	111.4(6)
C(7′)−N(5′)−Mn′	109.4(4)	C(6′)−N(5′)−Mn′	114.3(4)	N(2′)−C(20′)−C(15′)	107.2(5)	N(2′)−C(20′)−C(19′)	115.3(6)
N(1)−C(1)−C(2)	120.4(7)	N(1)−C(1)−C(21)	113.6(6)	C(15′)−C(20′)−C(19′)	110.4(6)	N(2′)−C(21′)−C(1′)	111.8(6)
C(2)−C(1)−C(21)	126.1(7)	C(1)−C(2)−C(3)	118.0(7)	N(2′)−C(21′)−C(23′)	109.9(6)	C(1′)−C(21′)−C(23′)	109.0(6)

[a] Symmetry transformations used to generate equivalent atoms.

pathways with ligand structure involves calculating, using molecular mechanics (MM), the energy of the Mn(III) complexes for all combinations of folding patterns and the corresponding energies associated with the Mn(II) structure containing the same folding pattern.[2] Another important aspect to this exercise is some knowledge of the orientation of the NHs relative to the substituents. For those complexes in which crystallographic data exists, the orientations are known. Thus, in the case of M40403 we observe that the NH pattern is alternating up−down−up−down.[10] Additionally, from the X-ray structure determination of the unsubstituted pyridine fifteen-membered ring complex, **9**,[3] we observe the same arrangement of NHs. Also, MM calculations on the five possible stereoisomeric arrangements reveal that the alternating up−down−up−down stereochemistry is the lowest energy for the both the Mn(II) complexes and the free ligands.[3] Using these data, certain structural relationships (e.g., a *trans*-cyclohexano substituent dictates that the NHs α to the substituted carbons of the macrocyclic ring must also be *trans*), and MM calculations for both the free ligands and for the Mn(II) planar seven-coordinate complexes, the NH pattern can be assumed with a high level of confidence for all of these complexes.

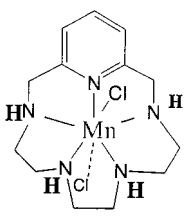

9

The goal of the modeling exercise with these pyridyl-bis-cyclohexyl substituted ligands is to ascertain the ability of the ligands to fold into a pseudooctahedral geometry about the Mn(II) ion by calculating the ΔE ($E_{Mn(III)} - E_{Mn(II)}$) for the most favorable fold, i.e., lowest energy folded structure. Another pertinent piece of data from the modeling would be structural prediction regarding which Cl−Mn−N bond angle in the six-coordinate structures will be the largest, i.e., predicting which N atom will fold. In this system of pyridine containing fifteen-membered ring ligands we observe in all our computations that the pyridine nitrogen and the two secondary amines adjacent to the pyridine are fixed to be in the same plane and will not afford a lowest energy folded structure. Thus, the two nitrogen atoms which reside on the chelate ring that is between the two fused cycohexano groups are the nitrogens which will in general be observed to provide the lowest energy folded structure.

For the complex M40403 there is only one unique folded structure as the two sides of the ligand are chemically identical. When M40403 is minimized as the six-coordinate structure, we observe that there is a tendency for the complex to fold one of the nitrogens between the two fused cyclohexyls into the vacant axial coordination site. In Figure 4 is shown the lowest energy six-coordinate Mn(II) structure available for all possible NH folding motifs and the corresponding six-coordinate Mn(III) pseudooctahedral structure for M40403. In Table 10 is a compilation of the calculated ΔE ($E_{Mn(III)} - E_{Mn(II)}$) values and the calculated bond angles defined by the axial ligand atom (chloro for convenience in all cases) and the Mn and the nitrogen atom most folded out of the plane defined by the Mn and the remainder of the four nitrogen atoms for M40403, **3**, **5**, and **6**. For M40403 the ClMnN angle is 114° and the ΔE is +1.2 kcal

Table 8. Atomic Coordinates [$\times 10^{+4}$] and Equivalent Isotropic Displacement Parameters [$\Delta^2 \times 10^{+3}$] for **5**

	x	*y*	*z*	*U*(eq)[a]
Mn	7393(1)	6295(1)	1433(1)	33(1)
Mn′	12065(1)	9414(1)	3255(1)	45(1)
C1(1)	5414(1)	6361(2)	279(1)	44(1)
C1(2)	9370(2)	6215(2)	2598(1)	48(1)
C1(1′)	10387(2)	9778(2)	2008(1)	54(1)
C1	14371(2)	9374(2)	4731(1)	50(1)
N(1)	6620(5)	6780(4)	2514(4)	35(2)
N(2)	7217(4)	8008(4)	1439(4)	34(2)
N(3)	8397(5)	6904(4)	484(4)	36(2)
N(4)	7797(5)	4929(4)	717(4)	34(2)
N(5)	6950(5)	4901(4)	2226(3)	34(2)
N(1′)	13200(5)	9157(5)	2373(4)	36(2)
N(2′)	11990(5)	7719(4)	2959(4)	36(2)
N(3′)	11838(5)	8860(4)	4484(4)	39(2)
N(4′)	11273(5)	10586(4)	4030(4)	35(2)
N(5′)	13021(5)	10864(4)	3224(4)	36(2)
C(1)	5994(6)	6130(6)	2859(4)	38(2)
C(2)	5566(6)	6396(6)	3560(4)	44(2)
C(3)	5742(6)	7349(6)	3869(4)	45(2)
C(4)	6352(6)	7999(6)	3517(4)	42(2)
C(5)	6799(5)	7693(5)	2831(4)	31(2)
C(6)	7543(6)	8307(5)	2389(5)	39(2)
C(7)	7785(6)	8537(5)	842(5)	36(2)
C(8)	7168(6)	9455(6)	435(5)	55(2)
C(9)	7769(7)	9953(6)	−187(5)	57(2)
C(10)	7923(7)	9272(6)	−909(5)	57(2)
C(11)	8511(6)	8332(5)	−502(5)	46(2)
C(12)	7886(6)	7830(5)	97(5)	34(2)
C(13)	8476(7)	6146(6)	−163(5)	49(2)
C(14)	8699(6)	5176(6)	282(5)	48(2)
C(15)	8032(6)	4081(5)	1307(5)	32(2)
C(16)	8165(6)	3119(5)	838(5)	44(2)
C(17)	8450(7)	2259(6)	1479(5)	57(2)
C(18)	7536(8)	2163(6)	1962(6)	70(3)
C(19)	7373(7)	3117(6)	2426(5)	52(2)
C(20)	7070(6)	3971(5)	1787(5)	37(2)
C(21)	5835(7)	5142(6)	2391(5)	51(2)
C(22)	7565(6)	9381(6)	2610(5)	52(2)
C(23)	5251(6)	4402(6)	2814(5)	64(2)
C(1′)	13222(6)	8275(6)	2015(5)	34(2)
C(2′)	13851(6)	8106(6)	1399(5)	44(2)
C(3′)	14375(6)	8885(7)	1128(5)	44(2)
C(4′)	14320(6)	9799(6)	1477(5)	45(2)
C(5′)	13735(6)	9918(6)	2127(4)	35(2)
C(6′)	13686(6)	10897(6)	2556(5)	40(2)
C(7′)	12232(6)	11685(5)	3207(5)	35(2)
C(8′)	12748(6)	12716(6)	3211(5)	49(2)
C(9′)	11833(8)	13492(6)	3190(6)	63(3)
C(10′)	11342(8)	13421(6)	3986(6)	73(3)
C(11′)	10863(7)	12379(5)	4037(5)	55(2)
C(12′)	11742(6)	11570(5)	4012(5)	42(2)
C(13′)	11239(7)	10246(5)	4909(5)	48(2)
C(14′)	10986(6)	9162(5)	4856(5)	45(2)
C(15′)	11779(6)	7582(5)	4438(4)	34(2)
C(16′)	12176(6)	7111(6)	5358(5)	51(2)
C(17′)	12210(7)	6002(6)	5301(5)	57(2)
C(18′)	12941(6)	5692(6)	4683(5)	50(2)
C(19′)	12477(6)	6120(5)	3780(4)	38(2)
C(20′)	12464(6)	7233(5)	3813(4)	34(2)
C(21′)	12487(7)	7452(6)	2232(5)	44(2)
C(22′)	14911(5)	11276(7)	2963(5)	62(2)
C(23′)	11526(7)	7209(6)	1395(5)	61(2)

[a] *U*(eq) is defined as one-third of the trace of the orthogonalized U_{ij} tensor.

with the Mn(III) structure at a slightly higher energy. The purpose of the modeling exercise is to probe the ease of folding by placing additional substituents on the ligand and determine how other substituents and their placement (position and stereochemistry) affect the ease of folding. A synthetically attractive family of substituted derivatives of M40403 is accessible by the use of the 2,6-diacetylpyridine affording after reduction the dimethyl substituted derivatives **3**, **5**, and **6.** The synthetic accessibility of these derivatives made them attractive initial targets for modeling. In Figures5−7 are shown the corresponding lowest energy six-coordinate structures and their Mn(III) folded structures for **3**, **5**, and **6**.

Table 9. Catalytic Rate for SOD Activity and Kinetic Stability of the New Complexes

complex	k_{cat} **(**pH=7.4**)** (M^{-1} s^{-1} x 10^{-7})	k_{diss} (M^{-1} s^{-1})
M40403	1.64	0.13
3	none detected	0.019
5	160	1.02
6	1.57	0.38

Table 10. The ΔE Values Calculated for the Lowest Energy Folded Structures and the Corresponding Calculated ClMnN Angle [deg] for the Mn(II) Complex.

compound	ΔE ($E_{Mn(III)} - E_{Mn(II)}$) (kcal**)**	∠ ClMnN **(**deg**)**
M40403	+1.2	114
3	+177	93.1
5	−3.0	124.6
6	+2.0	116.1

This MM calculational exercise reveals that the *trans-R,R*-isomer **3** is clearly constrained to a planar geometry of the macrocyclic ligand and as such would be predicted to be a very poor catalyst, as is observed. The extremely large energy difference ΔE of this complex is due to the very unfavorable energetics of folding the ligand into a constrained octahedral geometry as the Mn(III) complex. The cis-*R,S*-isomer, **6**, in contrast, appears to be similar to M40403 and in fact the bond angle of the folded nitrogen is very similar to the unsubstituted complex M40403. Since the ΔE is similar as well, we would predict that this *cis* complex **6** would have a catalytic profile similar to M40403. Indeed, we observe that M40403 and **6** have very similar catalytic rates. The modeling also predicts that the *trans-S,S*-complex **5** has a great propensity to fold as shown by the drop in energy when forced into the highly folded six-coordinate Mn(III) octahedral geometry and by the fact that the Mn(II) complex has the greatest degree of nitrogen folding from planarity with the ClMnN angle of 124.6°. Thus, modeling predicts that the *trans-S,S*-isomer **5** should be preorganized to fold to a greater extent and hence be a much better catalyst than M40403, **3**, or **6**.

The modeling results predict that the new complexes should also have a rank ordering of SOD catalytic activity as follows: **5** > **6** > **3**, as is observed (Figures 5−7). Clearly, one of the most striking results is that complex **3** has no measurable SOD catalytic activity. Since the modeling reveals that this Mn(II) complex is rigorously planar and possesses no tendency to fold, the observation of no detectable catalytic activity is consistent. That complex **5** has such favorable energetics of folding and is such a high activity catalyst is also consistent. The structure predicted for the six-coordinate Mn(II) complex of **5** from the MM calculations is also remarkably similar to the solid-state structure observed for the six-coordinate crystalmorph observed in the X-ray structure determination of **5** (Figure 7). Such details as the orientation of the methyl groups, the nitrogen which is folded, the orientation of NHs, and the alternating pattern of $C-CH_3$, CH, and NH orientations are identical between the observed and calculated structures. Additionally, the calculated ClMnN angle in the structure is 120.3°, while that calculated was 124°. The only observed difference between the calculated and observed structures is the orientation of the methylenes of the chelate ring, which is defined as the one

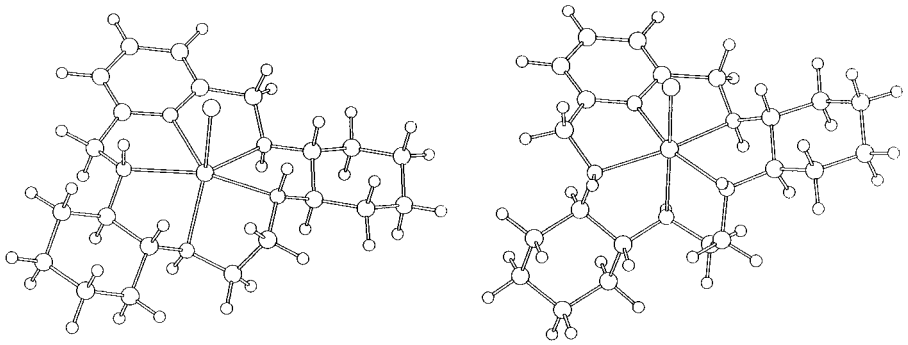

Figure 4. The lowest energy six-coordinate Mn(II) structure available for all possible NH folding motifs and the corresponding minimized six-coordinate Mn(III) pseudooctahedral structure for M40403.

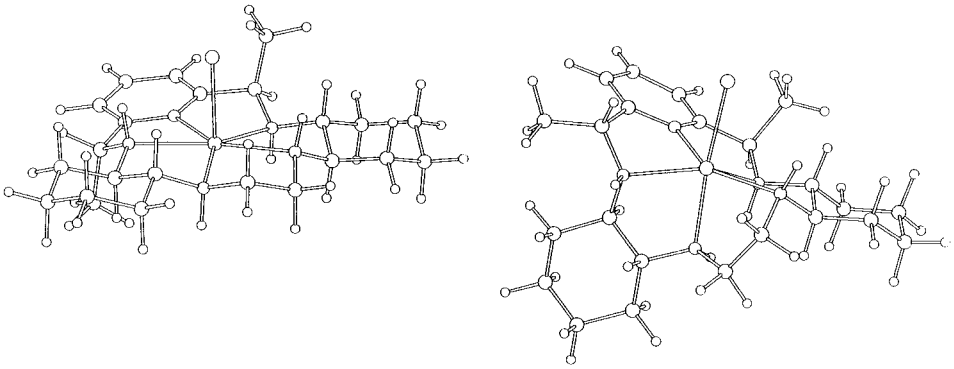

Figure 5. The lowest energy six-coordinate Mn(II) structure available for all possible NH folding motifs and the corresponding minimized six-coordinate Mn(III) pseudooctahedral structure for **3**.

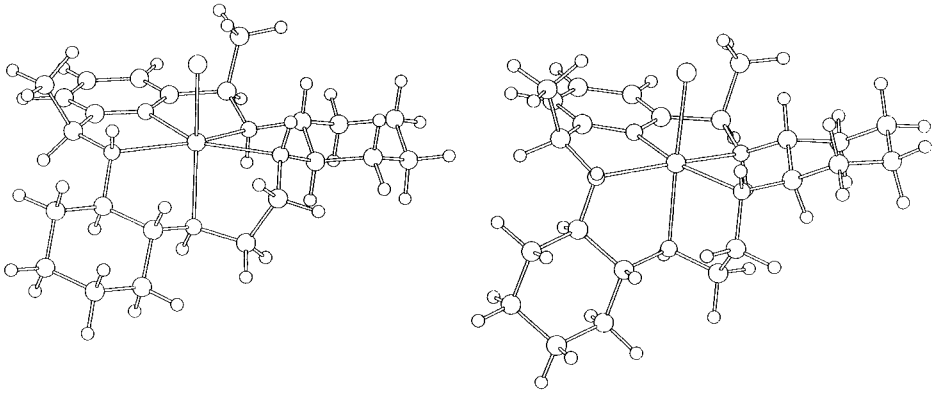

Figure 6. The lowest energy six-coordinate Mn(II) structure available for all possible NH folding motifs and the corresponding minimized six-coordinate Mn(III) pseudooctahedral structure for **6**.

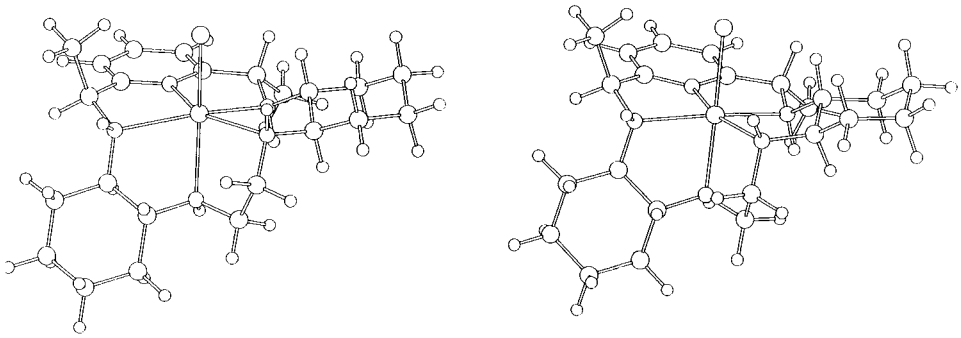

Figure 7. The lowest energy six-coordinate Mn(II) structure available for all possible NH folding motifs and the corresponding minimized six-coordinate Mn(III) pseudooctahedral structure for **5**.

between the two *trans*-fused cyclohexano rings, i.e., the one containing the folded NH.

Conclusions. Molecular mechanics (MM) calculations have made it possible to correctly predict how additional substituents and their stereochemistry will alter the catalytic activity of synthetic superoxide dismutase catalysts. The MM paradigm which we have developed has made it possible to design a family of stable, selective Mn-based SOD mimetics with

catalytic activities exceeding the native Mn SOD enzymes and with activities comparable to the Cu/Zn enzymes. The complex **5** possesses the highest catalytic rate for superoxide dismutation at pH = 7.4 of any known synthetic mimetic.[16] Further, as the complex **5** operates in a pH dependent ($HO_2^{\cdot}$ abstraction of a H atom of a bound water) mode unlike the natural enzymes, it actually increases in catalytic rate as the pH decreases. Thus at pH = 6.5 the catalytic rate for superoxide dismutation is $\sim 1 \times 10^{+10}$ M^{-1} s^{-1}—exceeding the rate of the native Cu/Zn SOD enzymes. At pH = 7.4 complex **5** is about 100 times more active than the M40403 complex which has previously been shown to be a very effective antiinflammatory compound in animal models of inflammation and reperfusion injury.[1] We have recently extended these in vivo animal studies to include complex **5** and find that the enhanced catalytic activity of complex **5** over M40403 translates into a much lower dose of compound to effect similar biological responses.[17] Thus, complex **5** exerts its protective antiinflammatory effects at approximately 100 fold lower doses; this is consistent with its enhanced catalytic rate.

Supporting Information Available: Tables listing the positional and isotopic displacement coefficients for hydrogen atoms and the anisotropic displacement coefficients for the non-hydrogen atoms are available for both structure determinations. This material is available free of charge via the Internet at http://pubs.acs.org.

IC000958V

(16) Riley, D. *Chem. Rev.* **1999**, *99*(9), 2573.

(17) (a) Cuzzocrea, S.; Calabrò, G.; Mazzon, E.; Costantino, G.; Caputi, A. P.; Riley, D. P.; Salvemini, D., *FASEB J.*, in press. (b) Cruzzocrea, S. *Shock* **2000**, *13*(1), 168. (c) Zweier, J. *Circulation*, 72nd Annual Meeting of the American Heart Association, November 7−10; Abs. 647.